scientific reports

Check for updates

OPEN

Laser surface texturing of glass with high-power picosecond laser for the control of optical properties

Dario Crimella[1], Tahseen Jwad[1], Andrea Bianco[2] & Ali Gökhan Demir[1]✉

The use of direct laser writing to manipulate the optical properties is an industrially appealing approach due to the high degree of geometrical flexibility provided by the approach. The recent introduction of high-power ultrafast laser sources renders this approach more productive with implications to move towards processing larger areas and faster processing times. The use of ps-long near infrared (NIR) pulses with high peak powers enables the processing of glass at the surface providing textures to manipulate the transparency and the refraction behaviour. This work proposes a systematic study to first define the feasibility window for surface processing of soda-lime glass with a high power ps-pulsed NIR laser, then generate different surface textures to vary the transmissivity and diffraction behaviour. The work shows the link between the inscribed texture, the surface roughness, and the different optical behaviours from diffractive to diffusive in the explored experimental conditions. The results show that the high power ps-pulsed lasers can effectively be used at several m/s scan speed levels to directly produce light diffusers or refractive optical elements.

Keywords Soda-lime glass, Surface texturing, Picosecond laser, Rear side damage, Optical diffuser

In the recent past, due to the development of new demanding applications, glass has gathered more attention thanks to its unique combination of properties such as its transparency within the UV-NIR spectrum, high hardness, corrosion resistance, chemical stability and electrical insulation[1]. Nowadays it is exploited in a wide variety of fields such as optics, photonics, displays, biomedical applications and many others[2,3]. However, because of its inherent properties, conventional machining of glass represents several challenges[4]. Therefore, nonconventional machining methods need to be utilized. Laser was proven to be a suitable machining method compared to the conventional ones, among which wheel cutting, abrasive waterjet, ultrasonic machining[3]. The main advantages of the laser technology, especially ultrashort pulsed lasers, are the absence tool wear, the extreme variety of feasible processes, the very high resolution and quality. Ultrashort pulsed lasers are preferred to continuous wave (CW) or nanosecond pulsed laser (ns) thanks to the reduced thermal effect and the better control of energy input that allow to have better quality and precision, thus making them the best choice for micromachining. Ultrashort lasers usually work in the visible and NIR range and the radiation absorption is made possible by nonlinear mechanisms induced by picosecond and femtosecond pulses[5,6]. This property gives high flexibility since it permits to focus the laser beam even through the substrate thickness. Indeed, bulk machining is used mainly for the production of the optical and photonic devices. Furthermore, surface structuring, drilling and cutting of glass are among the other processes that can be carried out employing ultrashort pulsed laser.

Surface machining is exploited to change the physical properties, such as wettability[7–9], conductivity, and the optical ones. Since glass is a transparent material, surface-relief type optical devices, like diffusers and diffraction gratings, can be fabricated through laser patterning. Optical diffusers[10] scatter light such that its spatial coherence is substantially reduced generating smooth spatial light distribution with the absent of the zero-order[11]. The surface morphology can be either periodic[12,13] or random[14–17]. They are widely used in LEDs, imaging systems, illumination, sensing, lasers and displays. In the case of surface-relief diffusers, there are many fabrication methods, such as replica moulding[18], photolithography[19], embossing[20], electrospraying[21] and laser texturing[14–17]. The latter represents an efficient and flexible option, in terms of feasible geometries and processable materials. By means of ultrashort lasers, direct writing is possible without the need of any additional component, such as chemical solutions[22–24] or additives[25] to etch glass or metal plates to induce plasma ablation (LIPAA)[17,26]. The effect of surface texturing on glass and other transparent medium to control diffraction and diffusion effects has been discussed in the literature[27–29]. In the meanwhile, the power levels available to the ultrashort pulsed lasers increase, their use in the industry for serial production becomes more appealing. To

[1]Department of Mechanical Engineering, Politecnico di Milano, Via La Masa 1, 20156 Milan, Italy. [2]INAF-Osservatorio Astronomico di Brera, Via Bianchi 46, 23807 Merate, Italy. ✉email: aligokhan.demir@polimi.it

authors' knowledge the use of several hundreds of Watts average power of picosecond pulsed lasers and a systematic work showing the processing regimes, the surface topographies, and the optical properties has not been proposed in the literature.

Accordingly, this work reports laser texturing of glass by means of a 180 W, 10 ps-pulsed NIR laser for the modification of optical properties aimed at display and electronic applications. The work aims to show in a systematic manner how the laser texturing process can be developed and exploited in a flexible manner for industrial processing. Initially, the interaction between laser and glass was investigated, by analysing the effects of fluence (F), scan speed (v), hatch distance (h) and pulse repetition rate (PRR). Once the suitable condition of surface machining was obtained, patterned surfaces were fabricated by changing pulse distribution and energy on the glass surface obtaining both diffusers and periodic diffractive elements. The optical properties of the devices were measured in terms of light transmittance, by considering the total, diffuse and specular intensities along the visible spectrum.

Results

Determination of laser-induced damage threshold

As a first step into the machining of glass by a high-power ultrafast laser source, it is necessary to study the behaviour of the material under single pulse irradiation, which is the basic condition for understanding laser-material interaction. The damage threshold is strictly related to the nonlinear condition of optical breakdown, wherein the material start to absorb the laser radiation, and it occurs when a certain critical density of plasma is achieved. By increasing the laser energy, the amount of ionized material increases, indicating the onset of damage as the glass starts to absorb light. At each microstructural modification of a transparent material there is an associated change in the refractive index.

The results are shown for surfaces of both sides of the glass sample (see Fig. 1a), since the presence of damage was detected on the two sides. More specifically, the observed damage threshold on the bottom surface (F = 15.7 J/cm^2) is lower than that on the top (F = 36.6 J/cm^2), with a spot dimension of 10 µm and 14.5 µm respectively. This behaviour is related to optical phenomena affecting the laser beam propagation through the glass, such as diffraction, internal reflection and interference[30], but also to the shift of the focal position toward the bottom surface once the laser passes through the glass, as the refractive index of the substrate is larger than that of air. Furthermore, there may be an additional issue about energy dissipation in air on the upper side, while the remaining energy is confined into the material when the beam interacts with the bottom surface[31]. The presence of damage on both sides at $F \geq 36.6$ J/cm^2 means that the generation of filament, a kind of elongated damage affecting all the thickness of the sample, is most likely to occur.

By looking at the two trends, the spot enlarges as the fluence increases and on the bottom side it is larger than the top one until F = 47 J/cm^2, meaning that the rear-side damage is more effective than the front-side one for fluences below that value. By increasing F, the larger absorption on the front surface and the presence of bulk damage limit the energy deposition on the bottom[31], allowing to have a larger damage on the upper side.

The morphology of the damage is different on the two sides as well and it changes according to the fluence. On the front side the spot is featured by a rougher central zone made of melted material and a surrounding ring, resulting from the dynamics of melting and re-solidification of glass flowing outside the centre of the irradiation. While on the rear side the spot looks darker may be attributed to a higher ablation removal efficiency. At high fluences the spot appears to be the union of three different circular regions, which may be due to higher energy

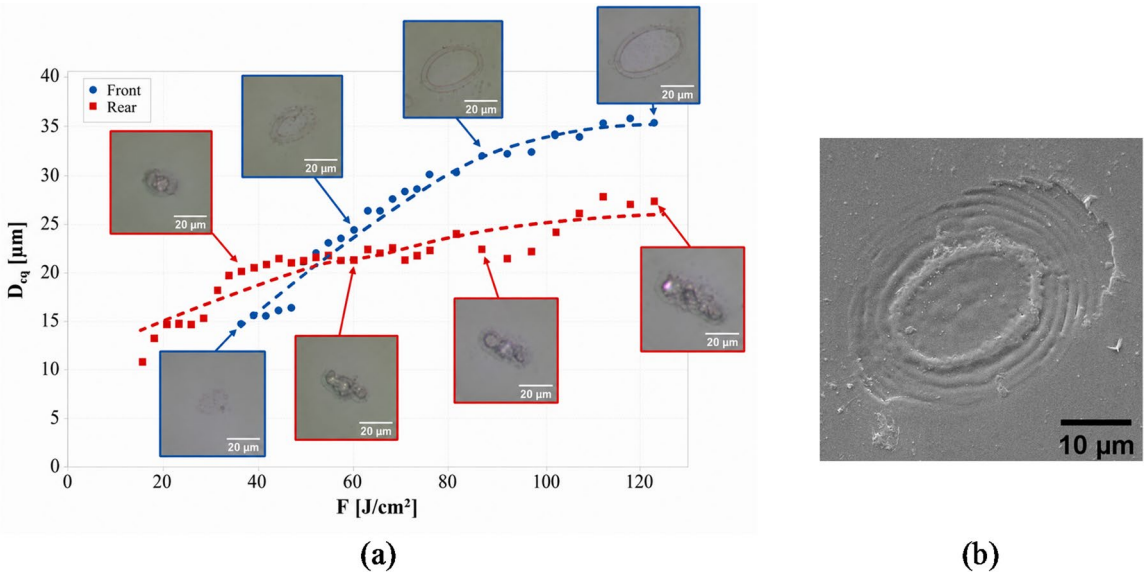

Fig. 1. (**a**) Dimension of irradiated area on both top and rear surface as a function of fluence. (**b**) SEM image of single ablated area on the front side at F = 130.5 J/cm^2.

had by the non-0th orders given by the beam diffraction. Furthermore, no presence of cracks was detected even at the highest fluence level.

With such a high level of pulse energy, the glass is ablated uniformly along the irradiated area. In some cases, wavy structures could be observed around the ablated region (see Fig. 1b). This phenomenon occurs in very few and randomly distributed spots, thus excluding any possibility of periodicity along the scanning path. The patterns were distributed radially with a periodicity of approximately 2 µm. As the employed laser had a linear polarization and the periodicity was observed to be larger than the laser wavelength, the formation behaviour is not expected to be linked to laser induced periodic surface structures (LIPSS). The observed periodic structures are more likely to be due to hydrodynamic behaviour of the molten glass rather than a surface interference phenomenon.

Overlapped pulse damage threshold

In multi-pulse condition, the damage generation is strongly related to the accumulation effect given by consecutive pulses. The fluence threshold (F_{th}) was determined experimentally by observing the minimum value that generates any damage on the surface. The fluence threshold decreases when the density of pulses per unit area increases, thus by reducing v or increasing PRR (see Fig. 2). The overall trends follow across different levels of PRR are found to be similar as they follow a hyperbolic increase. This is proof that both the spatial and temporal distances between consecutive pulses, controlled by v and PRR, respectively, affect energy accumulation. This accumulation is fundamental for inducing damage in the material, as it strongly influences material ionization and, consequently, the critical density. In terms of quality of the induced damage, the effect of the scan speed can be easily predicted: the faster the beam scanning, the farther apart are the irradiated spots, thus the lower are the heat accumulation and the probability to generate cracks and melt the material. The pulse repetition rate leads to a different consequence. An increase in the pulse repetition rate results in the laser-glass interaction becomes less stable. The obtained results show a lack of interaction continuity along the path and the presence of considerable cracks and melted material. The effect of PRR is enhanced at high v, meaning that increasing the speed is not necessarily beneficial for reducing the energy accumulated per unit area. Although higher speeds may reduce heat accumulation and the related detrimental effects, such as cracks and melted material, an excessive reduction of heat accumulation may weaken laser-material interaction and worsen process control.

Based on the achieved results, the best condition for glass machining, in terms of quality and controllability, consists of releasing pulses with high energy and low pulse repetition rate, thus large temporal distance between pulses. Although the focal position was set on the top surface, at 400 kHz damage occurrence was located on the bottom side, except for the case at the minimum scan speed. Rear-side damage occurred at low energies and low pulse repetition rates, indicating that higher energy input leads to faster achievement of the optical breakdown condition along the beam propagation direction.

Surface machining of soda-lime glass

Different processing regimes observed in areal scanning

The excessive heat input per unit time and the lack of control of laser-matter interaction occurring at high pulse repetition rate led to focus the surface machining analysis only at $PRR \leq 400$ kHz. In Figs. 3 and 4 the effects of fluence, scan speed and hatch distance are highlighted on both front and rear surfaces. With a fluence close to the damage threshold value, even though the damage is located on the rear surface only, no presence of cracks or chips can be noticed even with the lowest speed; while, by increasing the energy input, the heat effect is amplified,

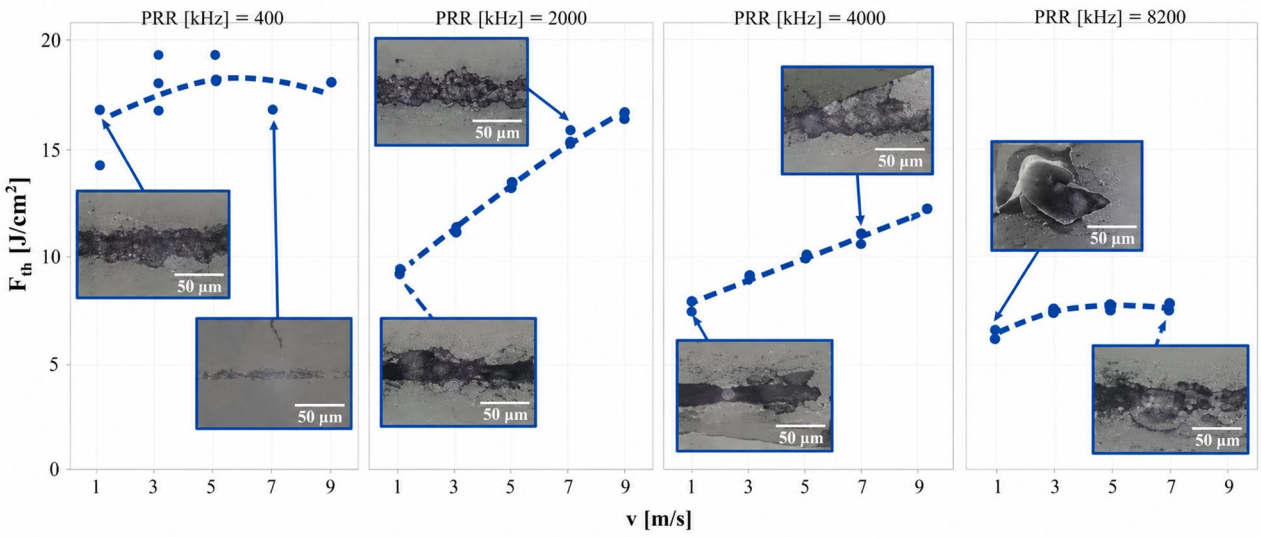

Fig. 2. Fluence threshold (F_{th}) with respect to scan speed and pulse repetition rate (dashed lines depict trend only).

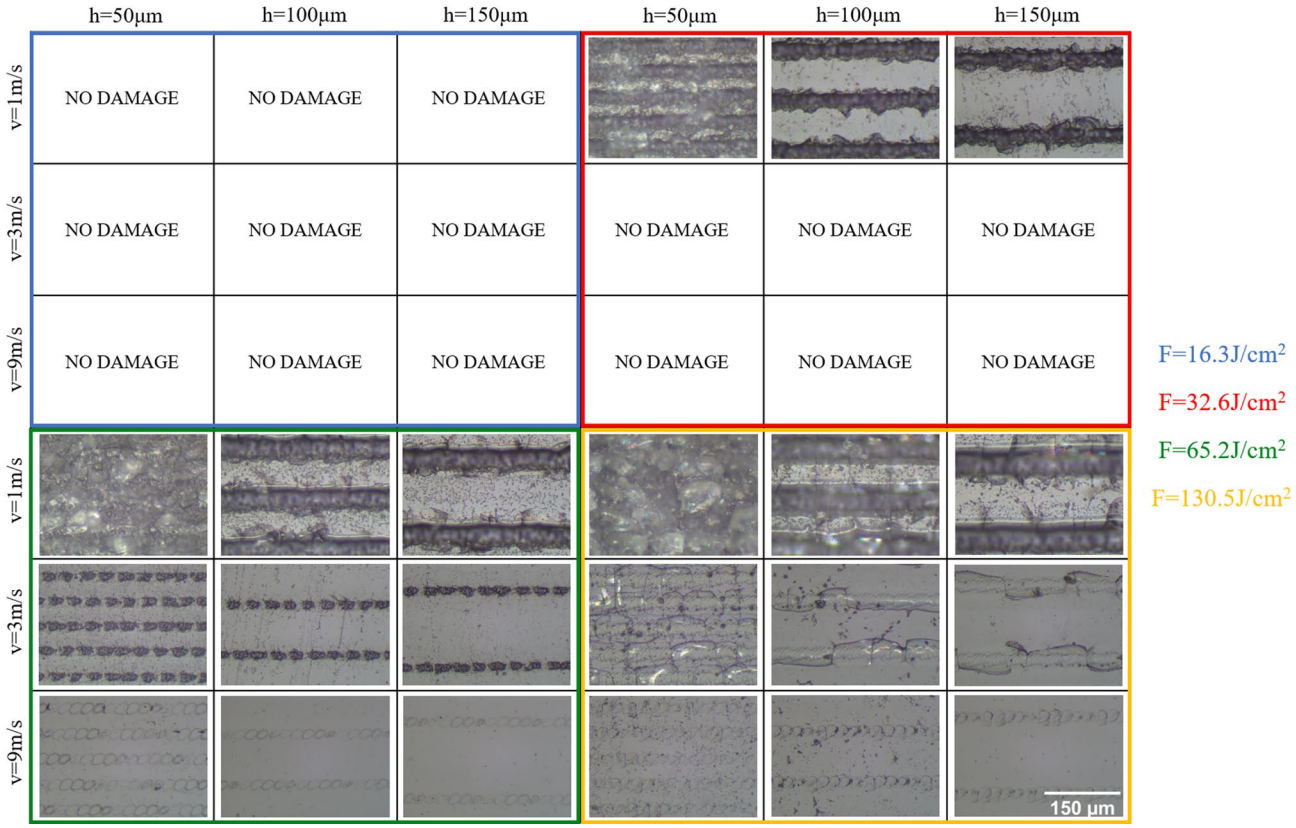

Fig. 3. Quality of front surface machining at 400 kHz as a function of fluence, scan speed, and hatch distance.

and it may be appreciated through the generation of both chips and cracks and the presence of melted material along the kerf edges. This effect is enhanced at low speeds because of heat accumulation across the material, while at high speeds the irradiation condition tends toward the single-pulse interaction. The hatch distance also plays a role in heat accumulation, although its effect is less pronounced. This is because the hatching lines are scanned unidirectionally, resulting in a longer elapsed time between consecutive heating phases, and the selected values of hatch distance are much larger than the groove width. Nevertheless, for large hatch distances the heat accumulation is confined around the kerfs. When decreasing the distance between lines, the propagation of chips and cracks through the grooves occurs and it may result in the damage of large portions of glass surface.

While working near the damage threshold, the damage is obtained only on the rear side for any combination of hatch distance and scan speed, because of the low energetic accumulation that allows the laser to pass through the glass without any consistent absorption on the front side. By increasing the fluence, for low scan speed the glass absorbs only on the front surface, while for high scan speeds the presence of damage on both sides may be detected. The heat accumulation on the rear side is in any case lower than on the front one because of the progressive light absorption of glass along the thickness.

To further study the rear-damage effect, an additional analysis was carried out at 100 kHz and maximum fluence (130.5 J/cm^2). To quantify the extent of the laser-glass interaction on both surfaces, the average surface roughness (S_a) was chosen as the representative parameter. With these specific values of pulse repetition rate and fluence, the damage can be seen on both surfaces; in this way, the effect of scan speed and hatch distance may be investigated. The SEM images (see Fig. 5) point out a similar trend of what shown previously (see Fig. 3) in terms of heat accumulation morphology and its detrimental effect on the glass surface. Observing the roughness measurements (see Fig. 6), both scan speed and hatch distance have an influence up to 3 m/s and 30 µm respectively, in particular on the rear surface. This is due to the dimension of the damaged area, which is around 35 µm on the front and 27 µm on the back; thus, once the spots are no longer overlapped, the surface roughness has little to no variation. As a general trend, the S_a values point out a more efficient damage on the back side but with less heat accumulation. This may be due to the lower laser intensity reaching the bottom of the sample and the shift in the focal position downwards once the laser passes through the glass, as already explained before. At low speed, it is possible to see that on the top side there is no considerable ablation of material but large heat accumulation, while on the back side kerfs down to 3 µm of depth are generated.

Modification of the optical properties of glass

The surface machining affects the optical properties of the glass according to the specific process parameters (see Fig. 7). By increasing the scan speed and the hatch distance, thus decreasing the pulse density, the surface structure changes from homogeneous to periodic. As a consequence, the transmitted light is diffused when the

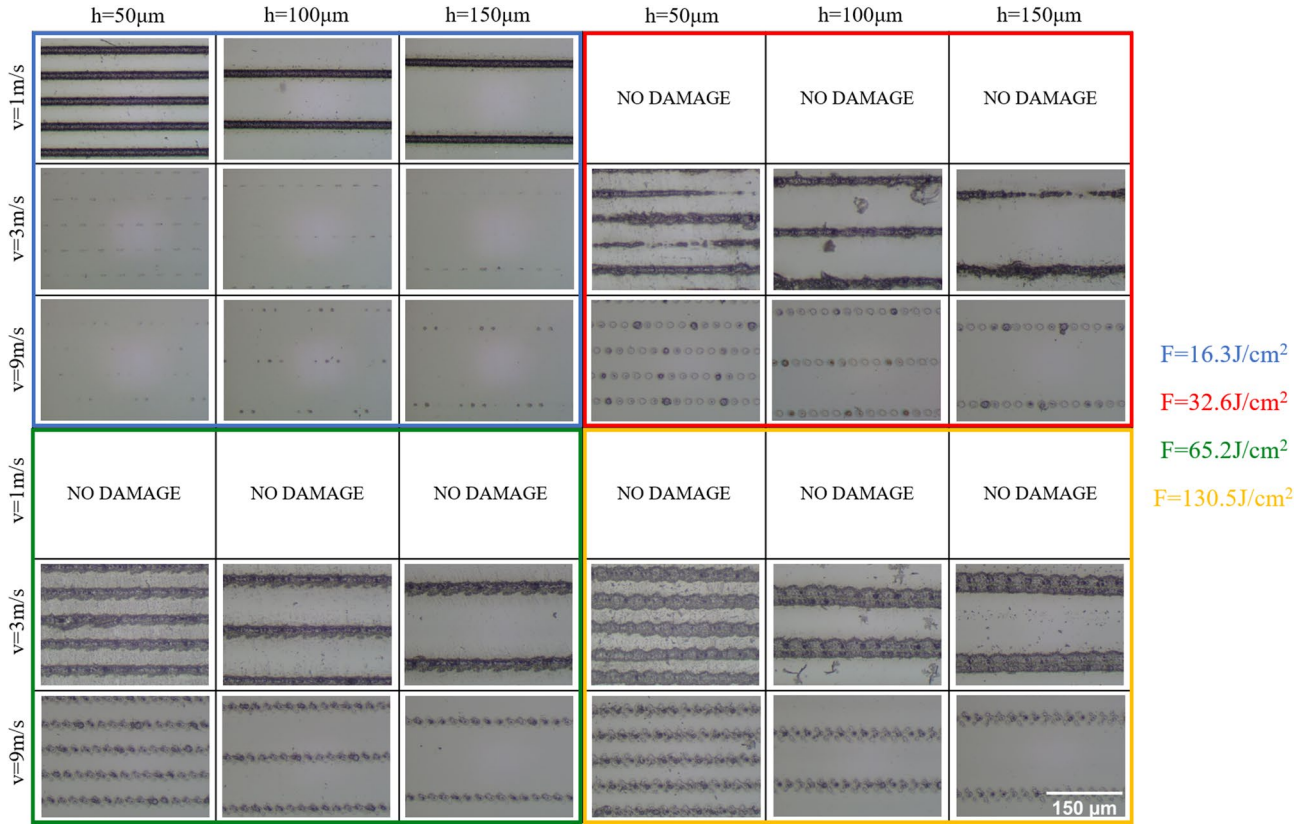

Fig. 4. Quality of rear surface machining at 400 kHz as a function of fluence, scan speed, and hatch distance.

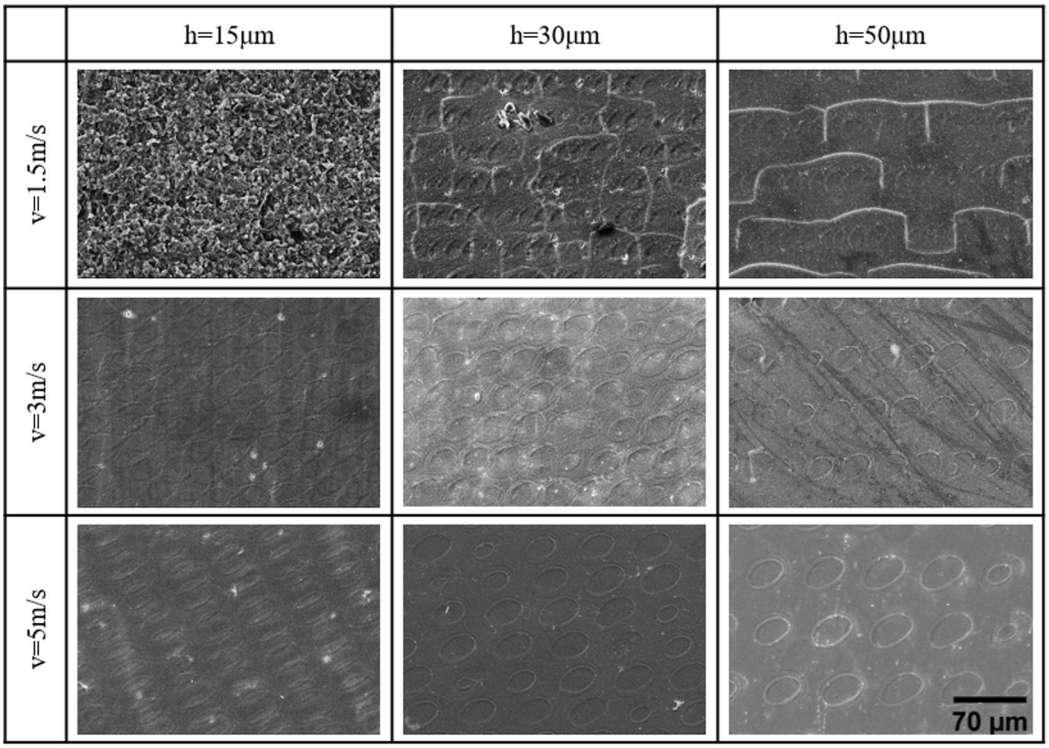

Fig. 5. SEM images of front surface morphology control through spatial overlap of pulses at $PRR = 100$ kHz and $F = 130.5$ J/cm^2.

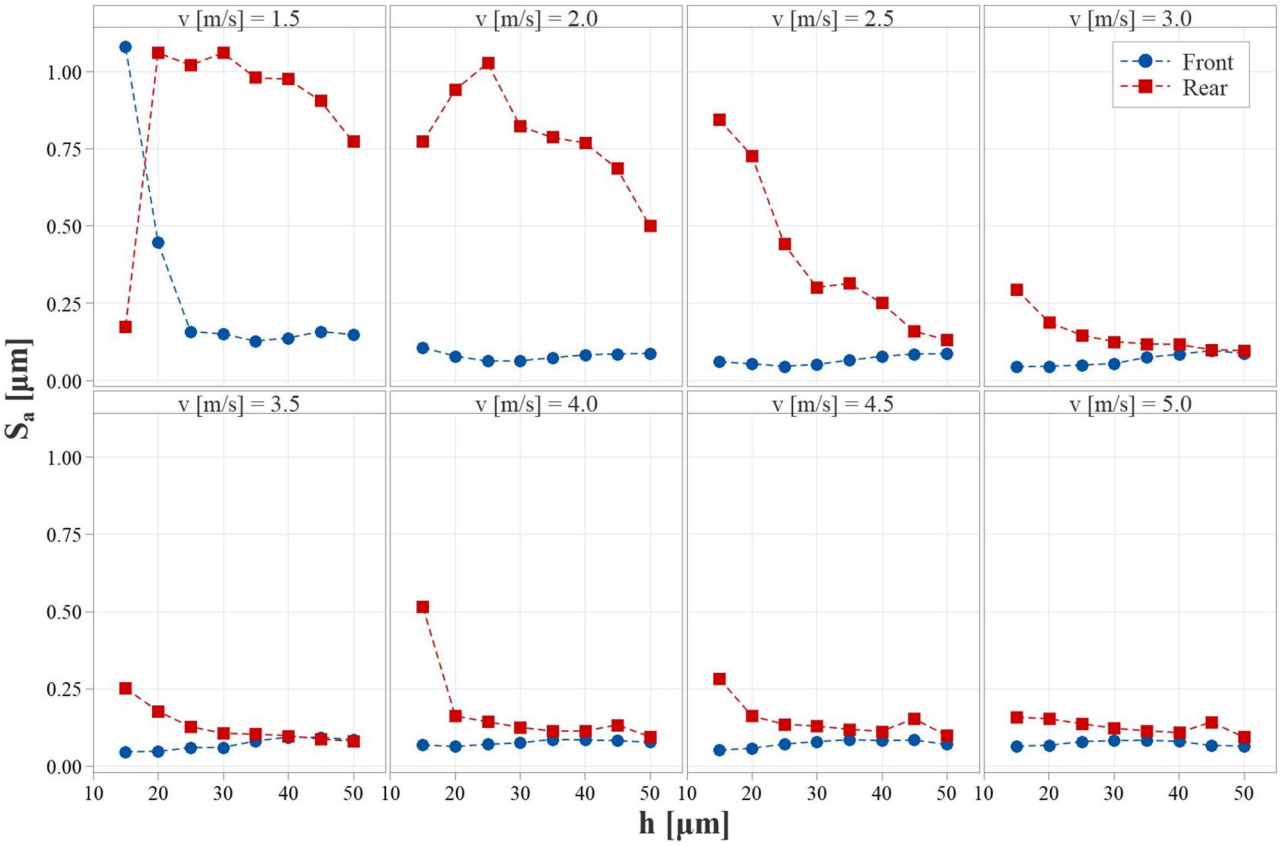

Fig. 6. Surface roughness as a function of hatch distance and scan speed on both front and rear side at PRR = 100 kHz and $F = 130.5$ J/cm^2 (dashed lines depict trend only).

pulse density is high, while it is diffracted when the written features are not overlapped in one or both directions thanks to the 1D or 2D periodicity. The fluence affects the surface structure as well, since the damaged area enlarges at higher fluence, thus enhancing the diffusive effect of glass. By looking at the total transmitted light shown in Fig. 8, it may be seen that it decreases with hatch distance, speed and fluence, thus when light diffusion is dominant. This happens because the surface structure becomes rougher and more homogeneous increasing the amount of scattered (diffused) light. The diffusive nature of glass at high pulse density and fluence can be proved by looking at the intensity of scattered light in Fig. 9, which is almost equal to the total one. According to Eq. (2), the specular contribution becomes almost negligible due to the large scattering effect (see Fig. 10).

By enlarging the pattern and decreasing the fluence, the light is less diffused and regular light patterns, typical of diffraction, by 2D periodic structures appears (see Fig. 7). The impact on the total amount of transmitted light is negligible as expected since a reflective grating is not promoted. Indeed, when the repeated surface features are relatively far from each other with respect to their size ($v \geq 5$ m/s and $h \geq 10$ µm), T_{tot} is almost constant at 91%, which is close to the specific value of non-machined glass. This means that the reflected light is only due to the Fresnel reflection losses (8.6% at 589 nm). The diffused intensity decreases with pulse density and fluence, while the specular contribution increases. Indeed, as T_{spec} reaches T_{tot}, the projected area becomes smaller until scattering is no longer considerable (see Fig. 7). This trend can be explained through the grating theory: as the distance between repeating elements increase, the diffraction angle reduces, thus the diffracted orders are confined in a more restricted area around the non-diffracted spot. A larger number of diffraction orders are visible and they become closer until they cannot be recognized anymore. Furthermore, as the wavelength decreases, the diffraction grating becomes more efficient, resulting in a higher T_{diff}. The process parameters employed for the study of light manipulation allowed to fabricate optical devices without the presence of any defects, such as cracks and melted material, on the surface of glass.

The effects of scan speed, hatch distance and fluence may be gathered into a single parameter, such as the surface roughness (S_a). In Fig. 11a, it is possible to appreciate the overall increase of the average surface roughness as the pulse density and the fluence grow. For high fluences, there is an optimal value of pulse density after which the roughness starts decreasing. This is due to the fact that closer interaction of the spots (high overlap) creates a more homogeneous surface, thus resulting in a lower S_a. The maximum S_a value achieved was ~1.9 µm. In Fig. 11b, the three different kinds of average transmittance are plotted as a function of the roughness. As it may be expected, the light diffusion increases as the surface becomes rougher, both for reflected and transmitted light. Therefore, the specular transmitted light decreases. The diffusive and the total transmission levels tend to move towards an asymptote at ~1.75 µm. In Fig. 11b, the diffusive and diffractive nature of the machined surface

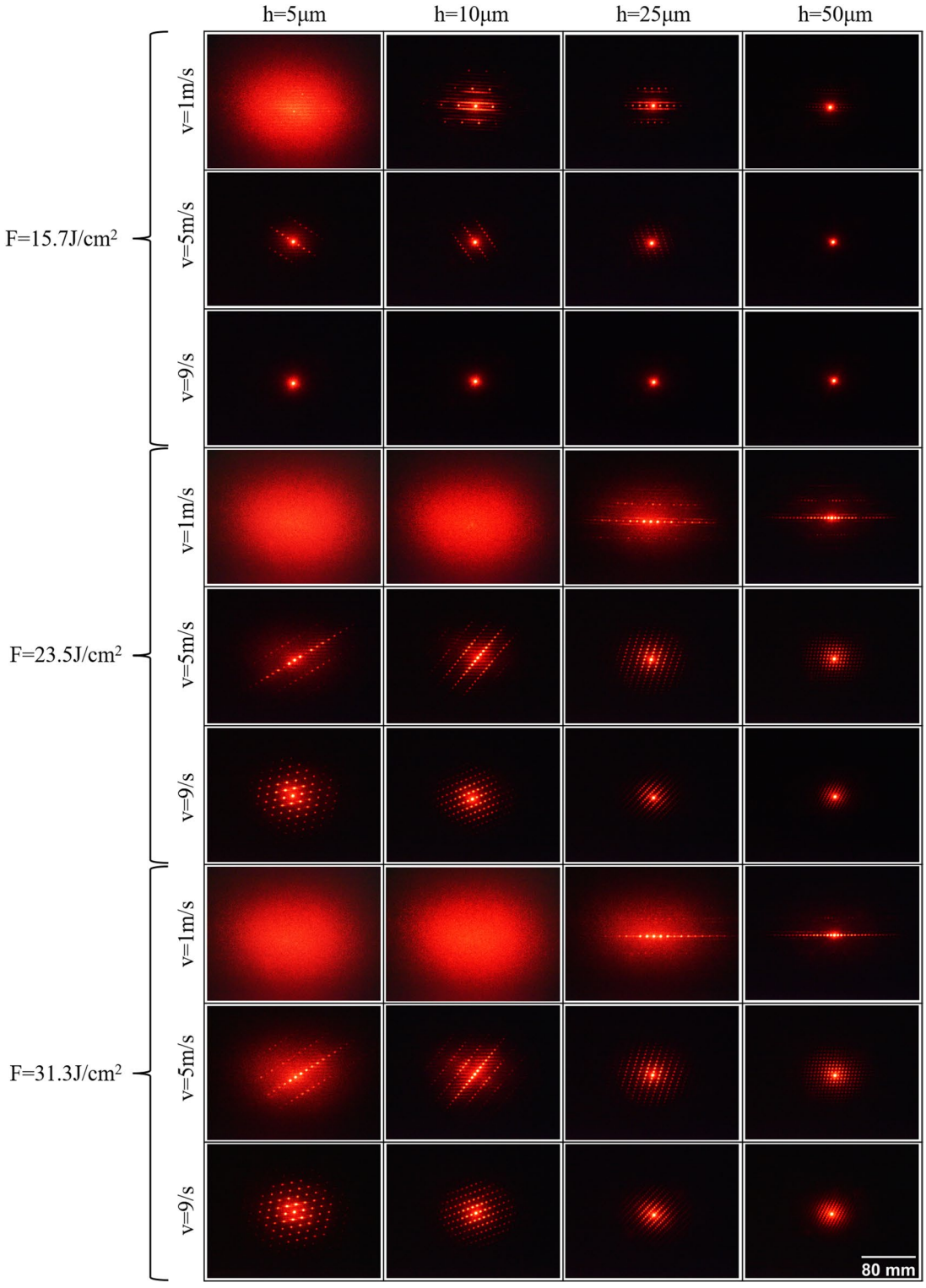

Fig. 7. Images of the light pattern projected as function of the working parameters. Diffusion and diffraction patterns at different levels of hatch distance, scan speed and fluence are visible.

is highlighted as well. There is no direct linear correspondence between the S_a value and whether the surface exhibits periodic diffractive features or uniform diffusive features. Ideally, the surface roughness and optical transparency should be controlled. The results imply that at low S_a values (< 0.25 μm) a reduction of specular transmittance and an increase of diffuse transmittance is present. Above this value the behaviour of specular and diffuse transmittance is relatively sparse. Indeed, light diffusion is a consequence of surfaces featured by homogeneous random microstructures and they are not necessarily rougher than periodic structures that cause

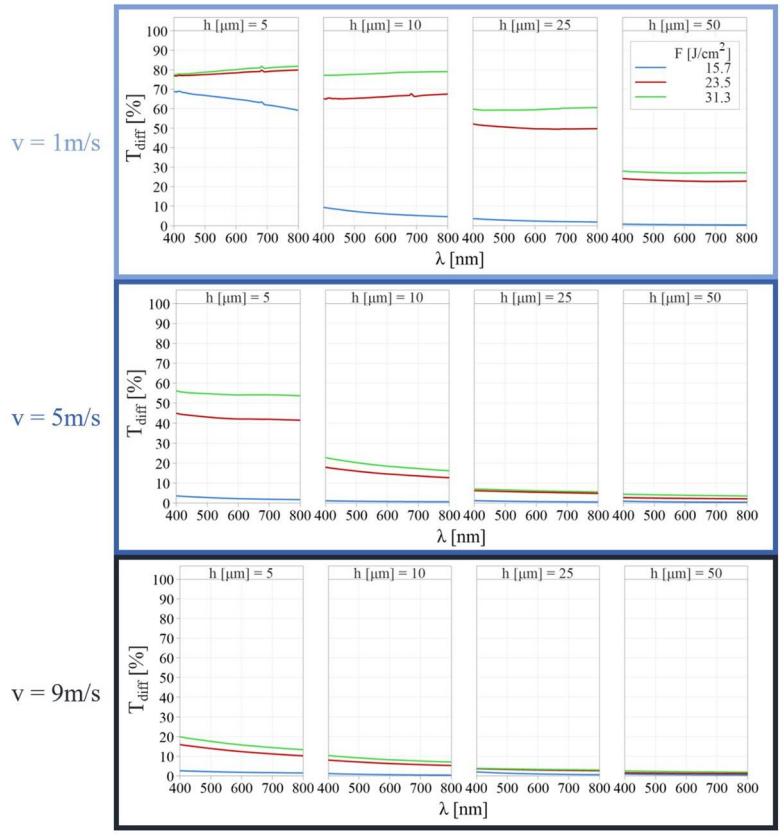

Fig. 8. Spectra of diffuse transmittance (T_{diff}) as a function of hatch distance, scan speed, and fluence.

diffraction. At low scan speed and large hatch distance, the machined surface shows grooves with a maximum depth of ~ 5 μm. At high scan speed and hatch distance, single pulses are visible on the surface having a depth as high as ~ 800 nm and a diameter as large as ~ 30 μm at maximum fluence.

Conclusions

In this work the surface machining of soda-lime glass through a high-power ps-pulsed NIR laser was studied, by focusing on the interaction between the radiation and the transparent substrate and the realisation of optical systems such as light diffusers and diffraction gratings. Concerning the investigated material-laser type combination, the following points can be listed as the main conclusions.

- Rear damage was observed during the experimental analysis. Several optical phenomena are expected to take place while the laser passes through the glass, such as focus shift, diffraction, internal reflection and interference, can be used to explain the effect. These effects are expected to reduce the damage threshold of the rear side compared to the damage threshold of the front side. Because of the lower threshold, the rear side machining is more effective, as also shown by the higher surface roughness on the bottom side.
- Glass machining at high pulse repetition rates reduced interaction stability by an increased thermal input. These conditions resulted in a non-homogeneous process featured by the presence of severe cracks and melted material. Increasing the scan speed was not found to be sufficient to mitigate the heat accumulation in the experimented range.
- In the stable processing conditions defect-free optical elements could be manufactured in a single-step process. The process parameters could be exploited to generate diffusive to diffractive elements. In particular, the total transmitted light was decreased and diffused light increased at higher pulse density and fluence.

Future works will be aimed at a deeper study of the filament creation occurring at low pulse repetition rates and high fluences. This kind of damage may be applied in glass cutting to achieve very high speeds by increasing the pulse repetition rate until an optimal value. The main application can be found in the display industry, but it may be exploited for cutting of thicker glass in order to replace the mechanical process currently used. Additional experiments about light manipulation can be carried out as well by focusing especially on optical diffusers, that can be optimised in diffusion angle and throughput according to the properties of the current laser setup. The chances to improve the productivity are high, again by increasing the pulse repetition rate. While the present work confirms the flexible use of ps-pulsed lasers to control optical properties further analysis of the optical performance is still required for a complete characterization required for the final applications. The use

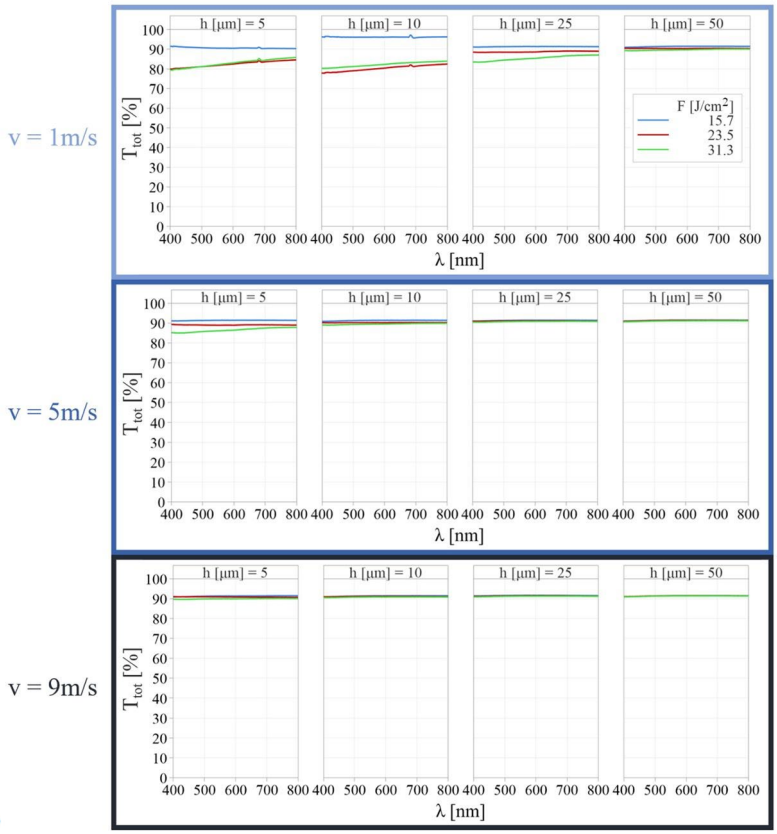

Fig. 9. Spectra of total transmittance (T_{tot}) as a function of hatch distance, scan speed, and fluence.

of simulation tools should also be exploited in the future for a greater understanding of the optical phenomenon involved in the process.

Methods

Material

The material used is 1 mm-thick soda-lime glass (76 × 26 × 1 mm^3 Marienfeld Superior UniMark microscope slides). This kind of glass is characterised by excellent thermal and optical properties and good machinability, making it widely used in many industrial applications. At 1064 nm, the material has an internal transmission T = 94.4%, a refractive index n = 1.5129 and an absorption coefficient α = 0.58 cm^{-1}[32].

High power ps-pulsed NIR laser

A picosecond-pulsed laser with 180 W nominal average power emitting at 1064 nm wavelength was used throughout the study (Lumentum Picoblade 3). The beam diameter in the focal position was calculated to be equal to 26.5 µm. The main specifications of the source are reported in Table 1. The output laser beam goes through an isolator (Electro-Optics Technology PAVOS isolator, 12 mm aperture), a beam expander (Jenoptik Beam-Expander) set to double the beam size, a series of two reflective mirrors to guide the laser beam into the scanner head (Raylase Superscan IV-20). For focusing, an f-theta lens with 163 mm of focal length (Jenoptik F-Theta JENar Silverline) was used. The focal position was controlled through a motorised vertical transitional stage and fixed on the top surface of the samples during the overall experimental activity.

Characterisation equipment

Optical microscopy (EchoLAB UM300I) was used to qualitatively assess the morphology and the quality of the machined surfaces, in terms of crack presence. Scanning electron microscopy (SEM, Zeiss EVO 50) was exploited for a deeper analysis of the interaction between laser and glass. Confocal microscopy (Mahr MarSurf CWM 100) was dedicated to surface roughness measurements. A spectrophotometer (Jasco V-770) equipped with a 60 mm integrating sphere (Jasco ISN-923) was used for the transmittance measurements.

Determination of laser-induced damage threshold

Laser-induced damage was initially characterized for single-pulses. The pulse energy (E) was varied throughout the experiments producing a range of fluences (F) between 10.4 and 122.7 J/cm^2. Optical microscopy was used to detect the presence of the damage caused by the laser interaction on both sides of the sample. Three measurements were taken for each combination. Later, the microscope acquisitions were processed through an

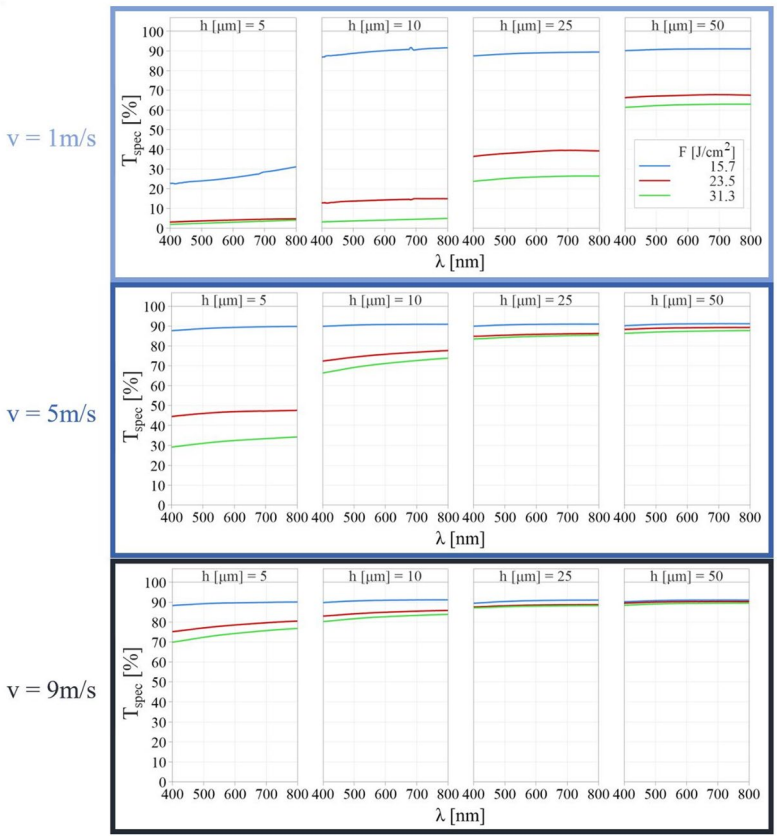

Fig. 10. Spectra of specular transmittance (T_{spec}) as a function of hatch distance, scan speed, and fluence.

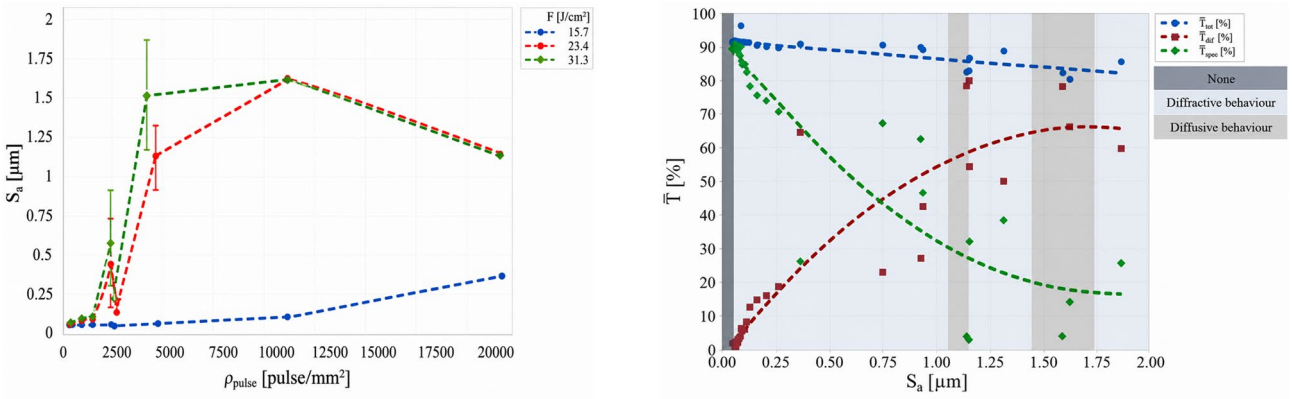

Fig. 11. (**a**) Surface roughness (S_q) as a function of pulse density and fluence (error bars represent one standard error from the mean and was calculated from the combinations producing the same pulse density, dashed lines connect mean values). (**b**) Average total ($\bar{T}_{tot}$), diffuse ($\bar{T}_{diff}$) and specular ($\bar{T}_{spec}$) transmittance as a function of surface roughness, where diffractive and diffusive behaviour regions are highlighted in different shades (dashed lines depict trend only).

image processing software (ImageJ) to measure the area of the spots (A_{meas}). The ablated region shape changed from circular to elliptical as the laser power increases, which is expected to be due to the beam shape and polarization[33], thus A_{meas} was converted into the diameter of an equivalent circle having the same area (D_{eq}), according to Eq. (1).

Parameter	Value
Pulse duration, t_{pulse} [ps]	10
Wavelength, λ [nm]	1064
Pulse repetition rate, *PRR* [kHz]	400–8200
Beam quality, M^2	1.2
Maximum average power, $P_{avg,\,max}$ [W]	180
Maximum pulse energy, E_{max} [μJ]	500
Maximum peak power, P_{peak} [MW]	39
Intensity distribution	Gaussian
Collimated beam size, d_c [mm]	5
Polarization	Linear horizontal
Focal length, f_{foc} [mm]	163
Focal diameter, d_0 [μm]	26.5

Table 1. Main specification of the laser system.

$$D_{eq} = \sqrt{\frac{4 \cdot A_{meas}}{\pi}} \tag{1}$$

Next, the damage therehsold study was extended to the linear scan condition, thus including the effect of additional process parameters such as pulse repetition rate (*PRR*) and scanning speed (v). The aim was to analyse the consequence of the heat input on the glass at different temporal and spatial distances.

For each combination of parameters, a raster of 8 mm-long lines was scanned by focusing the beam on the top surface. Through optical microscopy, the presence of damage in the material was detected. Three measurements were taken for each combination.

Identification of the feasibility window

Surface machining is achieved by adding the contribution of the hatch distance (h) as a process parameter, which represents the distance between consecutive parallel scanning lines. Based on the previous analyses, it was decided to focus on low *PRR*, while the levels of hatch distance were chosen to study the effect of crack propagation, if present, along and across the different lines. The following scanning technique was used: a 15×5 mm^2 raster of lines having a specific value of h and same scanning direction processed with one single pass. A single sample was produced for each combination considering the large experimental range. The processed samples were analysed through optical microscope for a qualitative assessment of the surface quality.

To better understand the causes of rear-damage and the influence of pulse overlap on glass absorption, the spatial overlap of laser pulses for a fixed dimension of the irradiated spot was studied by varying h and v. A low value of *PRR* was picked because of the detrimental effect related to a too short temporal distance between laser pulses but also considering the maximum speed exploitable with the current setup ($v_{max} \approx 12$ m/s), since the aim was to obtain an equal spacing of spots on vertical and horizontal directions by varying h and v within their limits, while the maximum energy level was used in order to accentuate the thermal nature of the laser-glass interaction and the glass absorption. The scanning technique was the same as the one previously reported.

Modification of the optical properties of glass

Surface texturing studied to the change of the optical properties of glass. In particular, the light transmission and the diffusive/diffractive behaviour in the visible spectrum were analysed as a starting point for the realisation of light-manipulation devices, such as large-scale optical diffusers and diffraction optical elements. Many levels of fluence, scan speed and hatch were used to obtain different conditions of pulse periodicity and damage. A measurement for each combination was made. The total (T_{tot}) and diffuse (T_{diff}) transmittance in the visible spectrum, from 400 to 800 nm, was measured by the spectrophotometer through the integrating sphere. The reference transmission spectrum was recorded by placing a Barium sulphate plate with 99.99% of reflectivity to close the integrating sphere. Considering that the glass does not absorb the light in the visible, only reflected light and transmitted light must be considered. Moreover, the total transmittance (T_{tot}) is given by the sum of two contributions, diffuse (T_{diff}) and specular (T_{spec}), and the latter is evaluated according to:

$$T_{spec} = T_{tot} - T_{diff} \tag{2}$$

The three parameters were also averaged along the overall spectrum (sampled every nm) according to:

$$\bar{T}_{tot/diff/spec} = \frac{\sum_{i=400}^{800} T_{tot/diff/spec}\,(i)}{401} \tag{3}$$

The simultaneous effect of scan speed and hatch is represented by the pulse density ρ_{pulse}, meant as the number of pulses shot per unit area:

$$\rho_{pulse} = \frac{PRR}{h \cdot v} \tag{4}$$

The surface roughness (S_a) was measured in order to gather the influence of all the variable parameters, such as scan speed, hatch and fluence. It was measured through confocal microscopy by considering a 0.3×0.5 mm^2 area at the centre of the processed surface.

To verify the light manipulation effect of the surface machined glass, a red laser was directed perpendicularly toward the sample and the result was projected on a black screen. The distance between the laser pointer and the glass sample was 45 mm, while the distance between the glass sample and the black screen was 403 mm.

Data availability

Data will made available upon reasonable request.

Received: 8 April 2026; Accepted: 26 May 2026
Published online: 03 June 2026

References

1. Axinte, E. Glasses as engineering materials: A review. *Mater. Des.* **32** (4), 1717–1732 (2011).
2. Ito, Y. et al. Precision cutting of glass by laser-assisted machining. *Int. Conf. Sustain. Mater. Process. Manuf. (SMPM 2017).* **7**, 240–245 (2016).
3. Ashkenasi, D. et al. Machining of glass and quartz using nanosecond and picosecond laser pulses. In *Laser Applications in Microelectronic and Optoelectronic Manufacturing (LAMOM) XVII*. (SPIE, 2012).
4. Nikumb, S. et al. Precision glass machining, drilling and profile cutting by short pulse lasers. *Thin Solid Films*. **477** (1–2), 216–221 (2005).
5. Liu, X., Du, D. & Mourou, G. Laser ablation and micromachining with ultrashort laser pulses. *IEE J. Quantum Electron.* **33** (10), 1706–1716 (1997).
6. Perry, M. D. et al. Ultrashort-pulse laser machining of dielectric materials. *J. Appl. Phys.* **85** (9), 6803–6810 (1999).
7. Ji, H. Y. et al. A simple approach to fabricate stable superhydrophobic glass surfaces. *Appl. Surf. Sci.* **266**, 105–109 (2013).
8. Wang, Z. et al. Glass surface micromachining with simultaneous nanomaterial deposition by picosecond laser for wettability control. *Appl. Surf. Sci.* **546** (2021).
9. Jagdheesh, R. et al. Laser-induced superhydrophobic and oleophobic surface structures on float glass. *Lasers Eng.* **50** (4–6), 289–298 (2021).
10. Zhou, L., Liu, S. J. & Zhong, T. J. A comprehensive review of optical diffusers: Progress and prospects. *Nanoscale* **15** (4), 1484–1492 (2023).
11. Höpe, A. Diffuse reflectance and transmittance. In *Spectrophotometry: Measurement of Optical Properties of Materials* vol 46, 179–219 (2014).
12. Alqurashi, T. & Butt, H. Highly flexible, stretchable, and tunable optical diffusers with mechanically switchable wettability surfaces. *ACS Central Sci.* **5** (6), 1002–1009 (2019).
13. Alqurashi, T. et al. Nanosecond pulsed laser texturing of optical diffusers. *AIP Adv.*, **7** (2) (2017).
14. Alqurashi, T. et al. Laser inscription of pseudorandom structures for microphotonic diffuser applications. *Nanoscale* **10** (15), 7095–7107 (2018).
15. Alqurashi, T. et al. Femtosecond laser directed fabrication of optical diffusers. *RSC Adv.* **7** (29), 18019–18023 (2017).
16. Murphy, K. et al. Holographic beam-shaping diffractive diffusers fabricated by using controlled laser speckle. *Opt. Express* **26** (7), 8916–8922 (2018).
17. Rong, W. K., Ando, K. & Nakajima, T. Facile fabrication of optical diffusers by ablation-assisted nanosecond laser micromachining of glass substrates. *Opt. Lasers Eng.* **167** (2023).
18. Wu, C. Y., Chiang, T. H. & Hsu, C. C. Fabrication of microlens array diffuser films with controllable haze distribution by combination of breath figures and replica molding methods. *Opt. Express* **16** (24), 19978–19986 (2008).
19. Yamashita, K. et al. Demonstration of a diffraction-based optical diffuser inspired by the butterfly. *Opt. Express* **29** (19), 30927–30936 (2021).
20. Bouchard, F., Soldera, M. & Lasagni, A. F. PMMA optical diffusers with hierarchical surface structures imprinted by hot embossing of laser-textured stainless steel. *Adv. Opt. Mater.* **11** (3) (2023).
21. Kim, G. H. & Park, J. H. A PMMA optical diffuser fabricated using an electrospray method. *Appl. Phys. A Mater. Sci. Process.* **86** (3), 347–351 (2007).
22. Kwon, K. K. et al. Precise glass microstructuring with laser induced backside wet etching using error-compensating scan path. *J. Mater. Process. Technol.* **291** (2021).
23. Kwon, K. K. et al. High aspect ratio channel fabrication with near-infrared laser-induced backside wet etching. *J. Mater. Process. Technol.* **278** (2020).
24. Niino, H. et al. Surface micro structuring of silica glass by laser-induced backside wet etching with a DPSS UV laser. *Appl. Surf. Sci.* **253** (19), 8287–8291 (2007).
25. Hopp, B., Vass, C. & Smausz, T. Laser induced backside dry etching of transparent materials. *Appl. Surf. Sci.* **253** (19), 7922–7925 (2007).
26. Hanada, Y. et al. Micromachining of transparent materials by laser-induced plasma-assisted ablation (LIPAA). In *Fifth International Symposium on Laser Precision Microfabrication*. Vol. 5662 (SPIE, 2004).
27. Heffner, H. et al. Surface modification of fluorine-doped tin oxide thin films using femtosecond direct laser interference patterning: A study of the optoelectronic performance. *Adv. Eng. Mater.* **25** (10) (2023).
28. Heffner, H., Soldera, M. & Lasagni, A. F. Optical enhancement of fluorine-doped tin oxide thin films using infrared picosecond direct laser interference Patterning. *Adv. Eng. Mater.* **24** (11) (2022).
29. Soldera, M. et al. Microfabrication and surface functionalization of soda lime glass through direct laser interference patterning. *Nanomaterials* **11** (1) (2021).
30. Russ, S. et al. Picosecond laser ablation of transparent materials. In *Laser-Based Micro- and Nanopackaging and Assembly* Vii, vol 8608 (2013).
31. Salleo, A. et al. Energy deposition at front and rear surfaces during picosecond laser interaction with fused silica. *Appl. Phys. Lett.* **78** (19), 2840–2842 (2001).
32. Rubin, M. Optical-properties of soda lime silica glasses. *Solar Energy Mater.* **12** (4), 275–288 (1985).
33. Stratakis, E. et al. Laser engineering of biomimetic surfaces. *Mater. Sci. Eng. R: Rep.* **141**, 100562 (2020).

Acknowledgements
The authors gratefully acknowledge the support of Lumentum for their collaboration and the technical support provided through this work. The authors acknowledge Raylase for the support provided.

Author contributions
DC and TJ have carried out the laser micromachining experiments. DC carried out optical microscopy, SEM, and surface roughness analyses. DC and AB executed the optical measurements and analysed the results. TJ and AGD conceptualized the work, designed the optical system and the experimental plans. AGD supervised the work. All authors contributed to writing and reviewing the manuscript.

Declarations

Competing interests
The authors declare no competing interests.

Additional information
Correspondence and requests for materials should be addressed to A.G.D.

Reprints and permissions information is available at www.nature.com/reprints.

Publisher's note Springer Nature remains neutral with regard to jurisdictional claims in published maps and institutional affiliations.

Open Access This article is licensed under a Creative Commons Attribution-NonCommercial-NoDerivatives 4.0 International License, which permits any non-commercial use, sharing, distribution and reproduction in any medium or format, as long as you give appropriate credit to the original author(s) and the source, provide a link to the Creative Commons licence, and indicate if you modified the licensed material. You do not have permission under this licence to share adapted material derived from this article or parts of it. The images or other third party material in this article are included in the article's Creative Commons licence, unless indicated otherwise in a credit line to the material. If material is not included in the article's Creative Commons licence and your intended use is not permitted by statutory regulation or exceeds the permitted use, you will need to obtain permission directly from the copyright holder. To view a copy of this licence, visit http://creativecommons.org/licenses/by-nc-nd/4.0/.

© The Author(s) 2026